AIAA JOURNAL
Vol. 33, No. 12, December 1995

# Aeroelastic Analysis of Multibladed Hingeless Rotors in Hover

Maeng Hyo Cho* and In Lee†
*Korea Advanced Institute of Science and Technology, Taejon 305-701, Republic of Korea*

**The coupled flap-lag-torsion aeroelastic response and stability of multibladed hingeless rotors in the hovering flight condition are investigated. The vortex lattice method, with a three-dimensional prescribed wake geometry, is used for the prediction of unsteady airloads of multibladed rotors undergoing disturbed dynamic motions. Interblade unsteady wake effects due to vortex-phasing phenomena beneath a rotor are numerically calculated by the phase control of wake vortices shed from each blade. The aeroelastic equations of motion of the rotor blade are formulated using a finite element beam model that has no artificial restrictions on the magnitudes of displacements and rotations due to the degree of nonlinearity. Numerical results of the steady equilibrium deflections and the lead-lag damping and frequency are presented for two-, three-, and four-bladed stiff-inplane rotors, and are compared with those obtained from a two-dimensional quasisteady strip theory with steady and uniform inflow.**

## Nomenclature

| | |
|---|---|
| $\boldsymbol{A}$ | = aerodynamic influence coefficient matrix |
| $a_0$ | = two-dimensional lift curve slope |
| $c$ | = blade chord length |
| $c_{d_0}$ | = profile drag coefficient |
| $\boldsymbol{G}(\boldsymbol{q}_0)$ | = gyroscopic damping matrix in finite element equation |
| $\boldsymbol{M}(\boldsymbol{q}_0)$ | = mass matrix in finite element equation |
| $m_0$ | = reference mass per unit length of blade |
| $N_b$ | = number of blades |
| $\boldsymbol{n}$ | = unit outward normal vector on the lifting blade surface |
| $\boldsymbol{P}(\boldsymbol{q}_0)$ | = internal elastic load vector in finite element equation |
| $\boldsymbol{P}_A(\boldsymbol{q}_0)$ | = generalized aerodynamic load vector in finite element equation |
| $\boldsymbol{P}_C(\boldsymbol{q}_0)$ | = centrifugal load vector in finite element equation |
| $\boldsymbol{q}_0$ | = generalized nodal displacement vector at steady equilibrium |
| $\tilde{\boldsymbol{q}}(t)$ | = small perturbation about steady equilibrium position $\boldsymbol{q}_0$ |
| $R$ | = blade radius |
| $\boldsymbol{V}$ | = kinematic velocity due to the blade motions |
| $\boldsymbol{W}$ | = induced velocity due to all wake vortices |
| $\Gamma$ | = bound vortex strength |
| $\gamma$ | = Lock number, $3a_0\rho_a cR/m_0$ |
| $\rho_a$ | = air density |
| $\psi$ | = dimensionless time, $\Omega t$ |
| $\Omega$ | = rotor angular velocity |
| $\omega_F, \omega_L, \omega_T$ | = nondimensional fundamental rotating flap, lead-lag, and torsion frequencies, respectively |

## Introduction

To perform a more reliable analysis of rotor aeroelastic stability, the use of an advanced rotary-wing aerodynamics with a sophisticated structural model is required, because aeroelastic stability is inherently a nonlinear phenomenon that involves structural, inertial, and aerodynamic loads. Recently, considerable effort and significant progress have been made with rotary-wing aeroelasticity.[1] Accurate modeling of the unsteady aerodynamic loads required for the aeroelastic response and stability calculations especially continues to be one of the major challenges facing both the analyst and the designer.

In realistic helicopter rotors, the aerodynamic environment of any rotor blade is strongly influenced by the passage of vortices shed from the preceding blades. A wake-excited flutter phenomenon was observed in experiments performed for hingeless[2] and bearingless[3] rotor blades. It has been established that the three-dimensional helical wake geometry beneath a rotor and unsteady wake dynamics effects are very important for aeroelastic stability of the rotor blade, as well as the prediction of helicopter performance.

In recent years, the panel method[4] and the vortex lattice method[5] for a three-dimensional prescribed wake geometry have been successfully applied to the aeroelastic response and stability of hingeless rotor blades in hover. Aeroelastic analysis[6] based on the generalized dynamic inflow model,[7] including a three-dimensional shed wake inflow, has also been performed. These studies have showed improved prediction of the lead-lag damping values over the full range of collective pitch angles, compared with results of two-dimensional quasisteady aerodynamics. The blade structural models used in these studies are conventional moderate deflection type beam theories[8,9] based on the ordering scheme that limits the magnitudes of displacements and rotations. The nonlinear aeroelastic equations of motion for these studies were formulated by Galerkin's method, based on the coupled rotating natural blade modes.

The finite element method has been extensively used in the rotary-wing aeroelastic problems because it is difficult to apply modal methods, such as Galerkin's method, to nonuniform blades and blades with complex root geometries. Furthermore, the finite element method is very flexible, and the formulation can be easily applied to various rotor blade configurations. The aeroelastic stability of rotor blades in hover has been investigated using the finite element method based on large deflection type beam theories,[10–13] as well as moderate deflection type beam theories.[14–16] However, the two-dimensional aerodynamic strip theory was used in these analyses.

In the present paper, the aeroelastic response and stability of multibladed hingeless rotors in hover are investigated using three-dimensional unsteady aerodynamics. The present three-dimensional aerodynamic model is the unsteady vortex lattice method representing a lifting surface and its wake by a number of quadrilateral vortex-ring elements. The three-dimensional wake geometry is prescribed from the known generalized equations.[17,18] The present method can predict the unsteady airloads of multibladed rotors and the effect of the interblade unsteady wake dynamics beneath the rotor blades on the aeroelastic response. A finite element beam model,[19] which is not based on an ordering scheme and includes all kinematically nonlinear effects, is used in this analysis. Transverse shearing deformations

Received Dec. 15, 1994; revision received May 25, 1995; accepted for publication May 25, 1995. Copyright © 1995 by the American Institute of Aeronautics and Astronautics, Inc. All rights reserved.

*Graduate Research Assistant, Department of Aerospace Engineering, 373-1 Kusong-dong, Yusong-gu.

†Associate Professor, Department of Aerospace Engineering, 373-1 Kusong-dong, Yusong-gu. Member AIAA.

and torsional warping effects are included in the formulation. The steady equilibrium deflections and the lead-lag damping values and frequencies are investigated for two-, three-, and four-bladed stiff-inplane rotors, which consist of the cantilevered rotor blades with uniform section properties. The results are compared with those obtained by the two-dimensional quasisteady strip theory studied in Ref. 20.

## Unsteady Vortex Lattice Method

As the rotor blade moves, vorticity is created in the boundary layers of the upper and lower surfaces, and vortices are formed along the sharp edges. These vortices are shed and convected away from the blade surface and constitute the wake. The wake beneath the rotor in hovering flight contains two primary components. The first is the strong tip vortex, which arises from the rapid rolling up of the portion of the vortex sheet shed from the tip region of the blade. The second is the vortex sheet shed from the inboard section of the blade.

In the present three-dimensional aerodynamic model, a lifting surface and its wake are discretized by a number of vortex-ring elements with piecewise constant strength, as depicted in Fig. 1. The tip vortex geometry is prescribed from Kocurek and Tangler's recirculation model[17] and the geometry of the inboard vortex sheet given by Landgrebe's model[18] is used.

In each panel of the blade surface, the leading segment of the vortex ring is placed on the panel's quarter chord line, and the collocation point is at the center of the three-quarter chord line. The boundary condition of no flow penetration on the lifting surface should be satisfied at the collocation point of each panel where the Kutta condition is satisfied implicitly. Thus, the following algebraic equations, in terms of the unknown circulation strength $\Gamma$ of the bound vortex, can be obtained[21]:

$$[A]\{\Gamma\}_{\text{blade}} = \{V \cdot n\} - \{W \cdot n\}_{\text{wake}} \tag{1}$$

where $[A]$ represents an aerodynamic influence coefficient matrix due to the unit strength bound vortex of each panel of the blade, $V$ the total kinematic velocity including the local surface velocity due to the elastic motion of the blade and the oncoming freestream velocity due to the blade rotation, and $W$ the total induced velocity contributed by all wake vortices. After obtaining the bound vortex strength $\Gamma$ of each panel at each time step, the local pressure difference can be computed by using the unsteady Bernoulli equation. The resulting sectional unsteady lift, induced drag, and pitching moment distributions about the aerodynamic center are then obtained by adding the contribution of the individual chordwise panels.

The motion of the multibladed rotor is generally described as a whole in the nonrotating frame instead of representing the motion of each blade separately in the rotating frame, since such a representation in the nonrotating frame simplifies both the analysis and understanding the behavior. To describe the motion of the rotor as a whole, dynamic interblade or nonrotating modes are introduced in the helicopter rotor dynamics (for more detail, see Ref. 22). For example, two-, three-, and four-blade rotors have two modes (collective and differential modes), three modes (collective, cyclic advancing, and cyclic regressing modes), and four modes (collective, differential, cyclic advancing, and cyclic regressing modes) in the nonrotating frame, respectively.

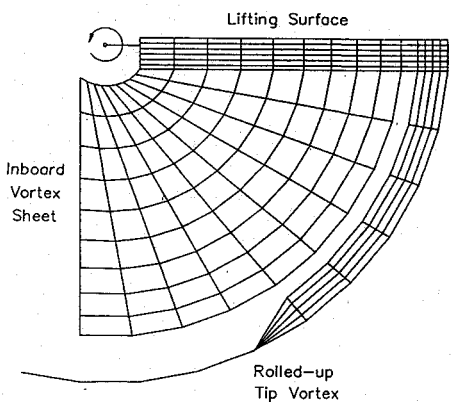


**Fig. 1 Numerical lifting surface and wake vortex panels.**

For an $N$-bladed rotor undergoing arbitrary transient motions, the wake-induced normal velocity term in Eq. (1) can be rewritten as follows:

$$\{W \cdot n\}_{\text{wake}} = \{W \cdot n\}_R + \{W \cdot n\}_{P1} + \{W \cdot n\}_{P2} + \cdots + \{W \cdot n\}_{P(N-1)} \tag{2}$$

where $R$ represents the reference blade, and $P1, P2, \ldots, P(N-1)$ represent the first, second, ..., $(N-1)$th preceding blades, respectively. In the present analysis, the interblade phase difference of all time-dependent shed vortices generated by the reference blade and the preceding blades undergoing different dynamic motions is considered by controlling the phases of the normal vectors of each panel on the blade surfaces, whereas interblade phase control was performed by the introduction of a phase control matrix in Ref. 23.

The position and orientation of the blade surface change from one time step to the next and, therefore, the aerodynamic influence coefficient matrix $[A]$ should be recomputed at every time step. The influence coefficient matrix, however, is computed only once for the steady equilibrium shapes of the deformed blade and the wake geometry because the unsteady motion of the blade is very small under the present small perturbation assumption. The zero normal flow boundary condition, however, should be updated at each time step.

The calculation of the steady loading is repeated until the converged solution of the whole vortex system is obtained for given blade configuration parameters, since the wake geometry is a function of the rotor thrust coefficient, number of blades, collective pitch angle, and blade twist. The unsteady loading is calculated through a time-marching solution procedure for small perturbed motions of the blade about the steady equilibrium position.

## Formulation and Solution Procedure

The blade structural model used in the present analysis is a finite element beam model developed in Ref. 19. The aeroelastic stability of hingeless rotor blades in hover, based on this model, has been investigated using the two-dimensional aerodynamic strip theory in Ref. 20. Thus, the following finite element equations of motion for a hingeless rotor blade can be obtained in the matrix form (for more detail, see Ref. 20):

$$[M(q)]\ddot{q} + [G(q)]\dot{q} + P(q) - P_C(q) = P_A(t, q) \tag{3}$$

To solve the governing equations of motion, the nonlinear steady-state deformation $q_0$ due to steady aerodynamic loads and centrifugal forces is first determined through the iterative Newton–Raphson method. The aeroelastic stability of a rotor blade is commonly investigated by linearizing the dynamics of the rotor blade about the nonlinear equilibrium position. The linearization of Eq. (3) cannot be expressed in explicit form, however, as in the two-dimensional aeroelastic analysis studied in Ref. 20, since the aerodynamic forces and moment are complex nonlinear implicit functions of the blade deformation and motion at each instant of time. Therefore, an ordinary eigenvalue analysis for determination of the stability is not possible. Thus, the linearized perturbation equations about the known equilibrium deflections $q_0$ can be reduced to the first-order ordinary differential equations of the following form:

$$\begin{Bmatrix} \dot{\tilde{q}} \\ \ddot{\tilde{q}} \end{Bmatrix} = \begin{bmatrix} 0 & I \\ -M^{-1}K & -M^{-1}G \end{bmatrix} \begin{Bmatrix} \tilde{q} \\ \dot{\tilde{q}} \end{Bmatrix} + \begin{Bmatrix} 0 \\ M^{-1}\tilde{P}_A \end{Bmatrix} \tag{4}$$

where $K = K_T - K_C$; $K_T$ and $K_C$ are the tangent matrices for $P$ and $P_C$, respectively; $\tilde{q}$ is the perturbed blade motion; $\tilde{P}_A$ is the perturbed load vector, which is calculated in real-time base from the input of $\tilde{q}$.

This system can be integrated numerically in time for the proper initial conditions of $\tilde{q}$, $\dot{\tilde{q}}$, and $\tilde{P}_A$. The initial value of $\tilde{q}$ is taken to be 10% of the equilibrium position $q_0$ (Ref. 4). The time is set equal to zero at the initial perturbation, and the blade is set free to move under the interaction of internal, inertial, and external aerodynamic loads. From the known values of the state vector and the perturbed aerodynamic loads, Eq. (4) is numerically integrated with

a fourth-order Runge–Kutta method. To obtain more accurate modal damping and frequency, the initial perturbation of the blade is given only in the particular mode of interest. Once the time histories of the blade lead-lag, flap, and torsional deflections are known, the modal damping and frequency of any desired mode can be determined from a moving-block analysis.[24] To reduce the computational time and the matrix size, a modal reduction through modal transformation is performed in the numerical integration procedure. Thus, the time history is calculated at the modal space, and the seven rotating normal modes[20] are used in this study.

## Discussion of Results

### Information for the Computation

In the present analysis, a simplified rotor blade with an untwisted rectangular platform is used to investigate the effects of the three-dimensional tip relief and the unsteady wake dynamics on the steady equilibrium deflections, the lead-lag modal damping, and frequency for multibladed rotors. Mass and stiffness properties along the span of the blade are assumed to be constant. The structural damping, blade precone and droop, and the pitch flexure are neglected. The chordwise offsets of the mass, tension, and aerodynamic centers from the elastic axis are also considered to be zero. The following configuration and operating condition parameters are used in the calculations:

$$\omega_F = 1.14, \quad \omega_L = 1.3, \quad \omega_T = 2.9$$
$$c/R = 0.09722, \quad N_b = 2, 3, 4 \qquad (5)$$
$$\gamma = 6.308, \quad a_0 = 2\pi, \quad c_{d_0} = 0.01$$

In the present vortex lattice method (VLM), the lifting surface is discretized by 6 chordwise × 14 spanwise vortex-ring elements, and the root cutout is 10% of the blade radius, as shown in Fig. 1. The dimensionless time step $\Delta\psi$ is 10 deg and the position of the rolled-up tip vortex is 60 deg. The wake is considered up to 720, 480, and 360 deg of the blade rotation for two-, three-, and four-bladed rotors, respectively, because the tip vortex geometry of Kocurek and Tangler's model[17] is used.

To verify the present VLM, the spanwise distribution of the normalized thrust loading for a two-bladed rigid rotor is compared with the experimental[25] and panel method's results[4] in Fig. 2. The present VLM gives accurate results, including the three-dimensional tip-loss effect.

In the following discussion of the results, the bending deflections in the lead-lag and flap directions are normalized with respect to the blade radius, and the torsional deflection is given in degrees. The lead-lag modal damping and frequency are normalized by rotor angular velocity. The results are also compared with those obtained from the two-dimensional aerodynamic strip theory. The induced inflow in the strip theory is taken to be steady and uniform along the blade span and equal to the value of nonuniform inflow given by combined momentum/blade element theory at the 75% spanwise station. Also, six four-noded beam elements are used, resulting in 108 degrees of freedom for the blade and providing reasonably good convergence for both static and dynamic analyses.

### Results

Figure 3 shows the equilibrium flap deflection at the blade tip for the two-, three-, and four-bladed stiff-inplane rotors. The lower flap deflections obtained by the three-dimensional theory (VLM) are due to the three-dimensional tip loss effect. Note that as the number of blades increases, the deflection decreases because of the decrease in the thrust loading. The equilibrium tip lead-lag deflection is represented in Fig. 4. The agreement between the predicted lead-lag deflections of two aerodynamic models is good at low collective pitch angles since the same profile drag coefficient is used. A difference in the results, however, appears at high collective pitch angles, since the two-dimensional theory gives overestimated induced drag. As the number of blades increases, the lead-lag deflection also decreases as the flap deflection does. Figure 5 shows the equilibrium tip torsion deflection for the two-, three-, and four-bladed rotors. It is observed that the torsion deflections predicted by the present VLM are about 30–40% of those given by the two-dimensional theory. This is due to the three-dimensional aerodynamic tip effect, which produces high nose-up pitching moment as discussed in Ref. 4. The effect of the number of blades on the torsion deflection is relatively small compared with two cases in the bending deflections.

The time histories of the lead-lag perturbed motions obtained from an initial perturbation of the lead-lag direction are shown in Figs. 6, 7, and 8 for the two-, three- and four-bladed stiff-inplane rotors, respectively. The results for the dynamic interblade modes (for example, collective and differential modes for two-bladed rotor) using the present unsteady vortex lattice method (UVLM) are compared with those given by the two-dimensional quasisteady aerodynamics. Since the same structural model is used for both two- and

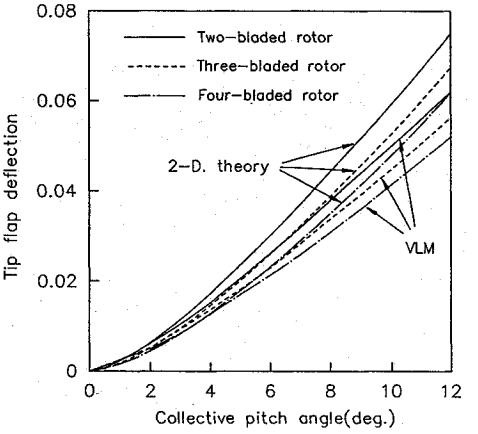


**Fig. 3 Equilibrium tip flap deflection of two-, three-, and four-bladed rotors.**

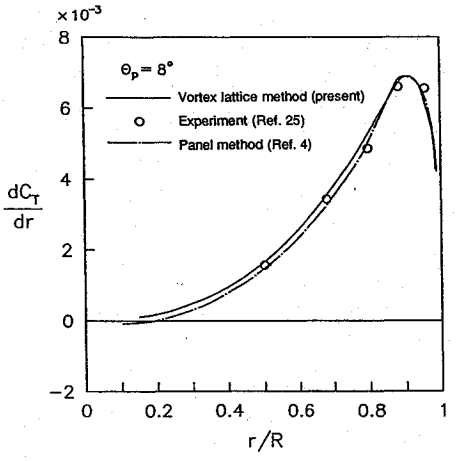


**Fig. 2 Spanwise thrust loading of a two-bladed rigid rotor, $AR$ = 6.**

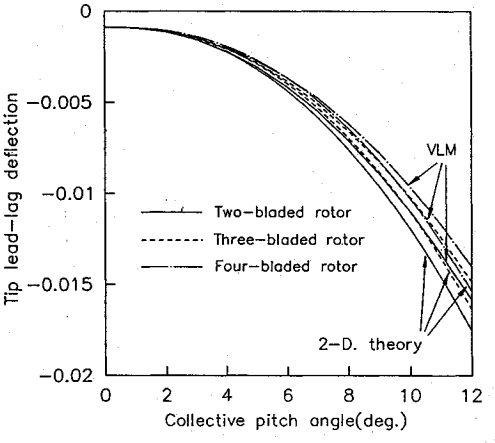


**Fig. 4 Equilibrium tip lead-lag deflection of two-, three-, and four-bladed rotors.**

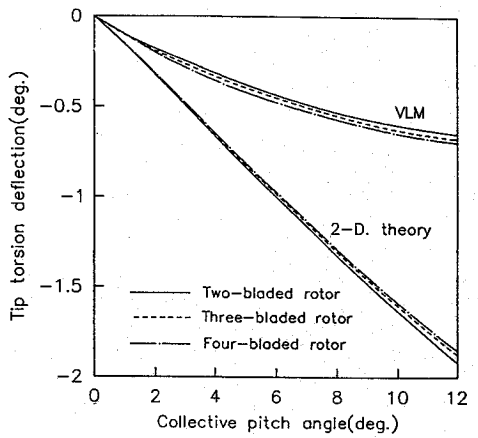


**Fig. 5 Equilibrium tip torsion deflection of two-, three-, and four-bladed rotors.**

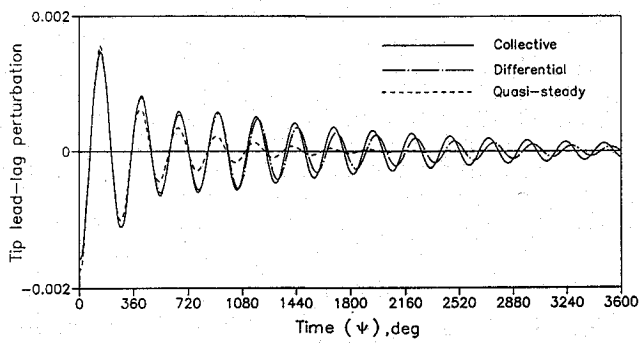


**Fig. 6 Time history of lead-lag perturbation obtained from an initial perturbation of lead-lag at 12-deg collective pitch angle for a two-bladed rotor.**

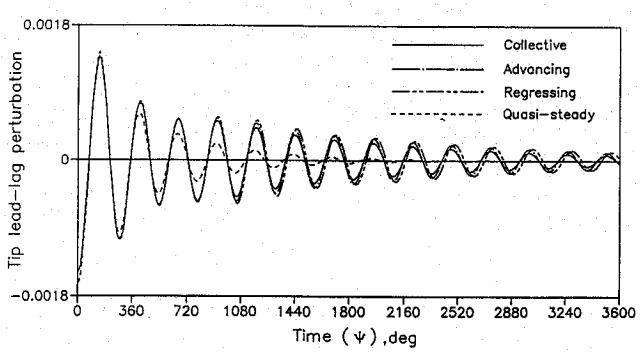


**Fig. 7 Time history of lead-lag perturbation obtained from an initial perturbation of lead-lag at 12-deg collective pitch angle for a three-bladed rotor.**

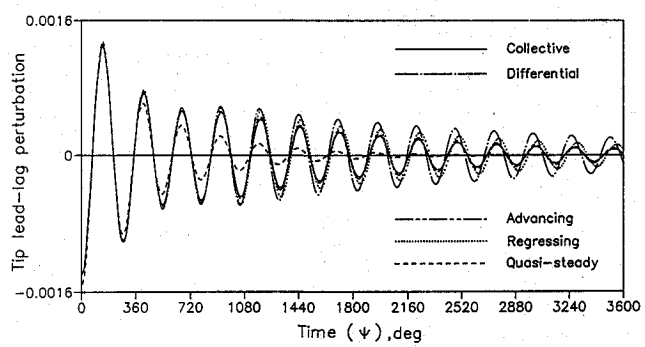


**Fig. 8 Time history of lead-lag perturbation obtained from an initial perturbation of lead-lag at 12-deg collective pitch angle for a four-bladed rotor.**

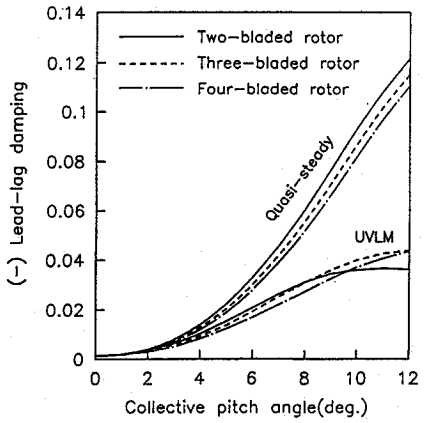


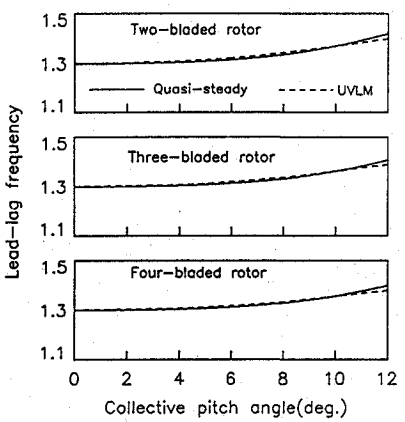


**Fig. 9 Lead-lag damping and frequency for collective modes of two-, three-, and four-bladed rotors.**

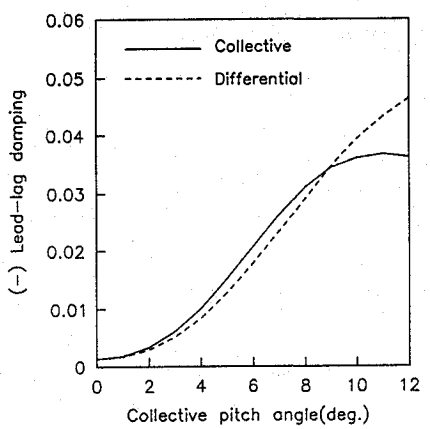


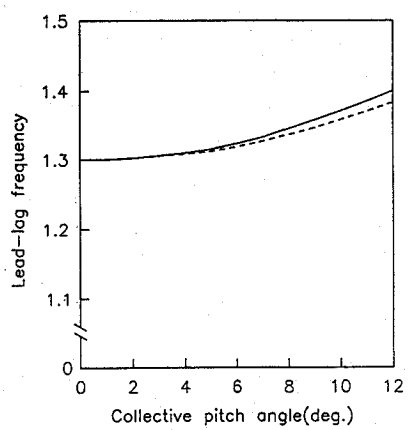


**Fig. 10 Lead-lag damping and frequency of a two-bladed stiff-inplane rotor.**

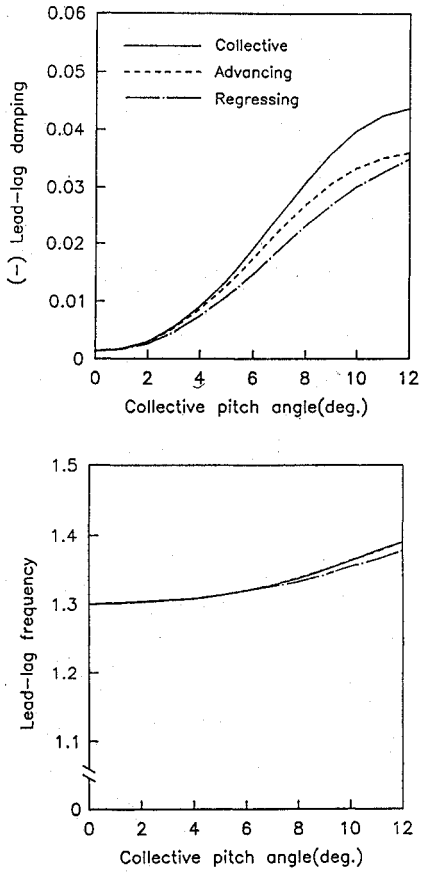


**Fig. 11 Lead-lag damping and frequency of a three-bladed stiff-inplane rotor.**

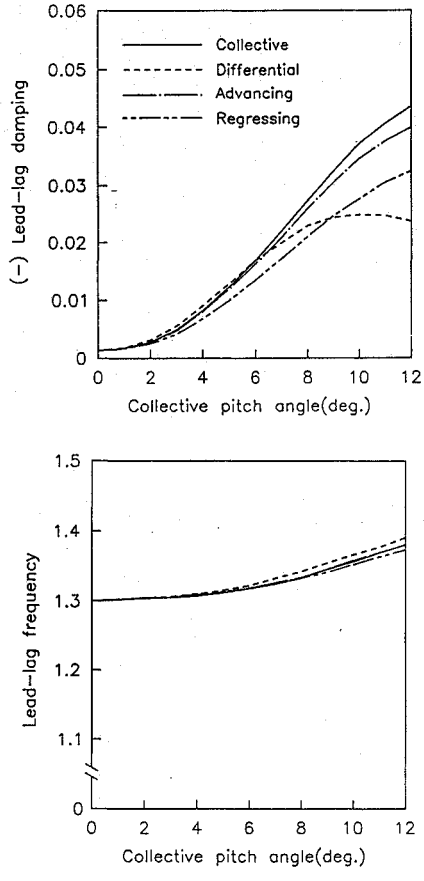


**Fig. 12 Lead-lag damping and frequency of a four-bladed stiff-inplane rotor.**

three-dimensional aeroelastic responses and there exists no structural damping, the difference between the results is due to different aerodynamic behavior. It is observed that as the number of blades increases, the time responses of the interblade modes become various and complex because of the interblade vortex-phasing effect of time-dependent wake vortices shed from all blades. In any case, the two-dimensional quasisteady aerodynamics gives inaccurate results at high collective pitch angles.

Predicted lead-lag damping and frequency for collective modes of two-, three-, and four-bladed rotors are shown in Fig. 9. The results of UVLM are obtained through a moving-block analysis, whereas the results of two-dimensional quasisteady theory are based on the eigenvalue analysis. At high collective pitch angles, it is shown that the lead-lag damping values obtained by the three-dimensional theory are about 40% of the damping obtained by the two-dimensional theory. This overprediction of the lead-lag damping by the two-dimensional aerodynamics is due to the lack of both three-dimensional tip and unsteady wake dynamic effects. The lead-lag frequencies obtained by two aerodynamic theories have a slight difference at high collective pitch angles, but those are almost identical.

The effect of the unsteady wake inflow dynamics due to the interblade vortex-phasing phenomena on the lead-lag damping and frequency are given in Figs. 10, 11, and 12 for two-, three- and four-bladed rotors, respectively. It is found that time-dependent shed vortices greatly affect the lead-lag damping of the hingeless stiff-inplane rotor in hover. In particular, the damping values for collective mode of the two-bladed rotor (Fig. 10) and differential mode of the four-bladed rotor (Fig. 12) are very sensitive to the collective pitch angles. The lead-lag frequencies, however, are not affected significantly by the different unsteady wake inflow dynamics.

## Conclusions

The aeroelastic analysis of multibladed hingeless rotor blades in hover has been performed using the vortex lattice method with a realistic wake structure that accounts for the three-dimensional aerodynamic tip relief and the unsteady wake inflow dynamics. The aeroelastic equations of motion of the rotor blade are formulated using a finite element beam model, where no restrictions are made on the magnitudes of displacements and rotations but the strains are assumed to be small compared with unity. The steady equilibrium deflections, the lead-lag damping and frequency for two-, three-, and four-bladed stiff-inplane rotors are compared with those obtained from the two-dimensional aerodynamic strip theory. The results show that the three-dimensional tip and realistic wake effects greatly affect the steady equilibrium and the rotor stability. It is especially found that the unsteady wake inflow dynamics effect due to the interblade vortex-phasing phenomena plays an important role in the lead-lag stability of multibladed hingeless rotors in hover.

## References

[1]Friedmann, P. P., "Rotary-Wing Aeroelasticity with Application to VTOL Vehicles," *Proceedings of the AIAA/ASME/ASCE/AHS/ACS 31st Structures, Structural Dynamics, and Materials Conference* (Long Beach, CA), AIAA, Washington, DC, 1990, pp. 1624–1670 (AIAA Paper 90-1115).

[2]Anderson, W. D., and Watts, G. A., "Rotor Blade Wake Flutter—A Comparison of Theory and Experiment," *Journal of the American Helicopter Society*, Vol. 21, April 1976, pp. 32–43.

[3]Bousman, W. G., and Dawson, S., "Experimentally Determined Flutter from Two- and Three-Bladed Model Bearingless Rotors in Hover," *Journal of the American Helicopter Society*, Vol. 31, July 1986, pp. 45–53.

[4]Kwon, O. J., Hodges, D. H., and Sankar, L. N., "Stability of Hingeless Rotors in Hover Using Three-Dimensional Unsteady Aerodynamics," *Journal of the American Helicopter Society*, Vol. 36, April 1991, pp. 21–31.

[5]Yoo, K. M., Hodges, D. H., and Peters, D. A., "An Interactive Numerical Procedure for Rotor Aeroelastic Stability Analysis Using Lifting Surface," *Proceedings of the 18th ICAS Conference* (Beijing, PRC), 1992, pp. 1272–1280 (ICAS-92-6.6.3).

[6]de Andrade, D., and Peters, D. A., "Correlations of Experimental Flap-Lag-Torsion Damping—A Case Study," Proceedings of the 49th Annual National Forum of the American Helicopter Society, St. Louis, MO, May 1993.

[7]Peters, D. A., Boyd, D. A., and He, C. J., "Finite-State Induced Flow Model for Rotors in Hover and Forward Flight," *Journal of the American Helicopter Society*, Vol. 34, Oct. 1989, pp. 5–17.

[8]Hodges, D. H., and Ormiston, R. A., "Stability of Elastic Bending and Torsion of Uniform Cantilever Rotor Blade in Hover with Variable Structural Coupling," NASA TN D-8192, April 1976.

[9]Hodges, D. H., "Nonlinear Equations of Motion for Cantilever Rotor Blades in Hover with Pitch Link Flexibility, Twist, Precone, Droop, Sweep, Torque Offset, and Blade Root Offset," NASA TM X-73,112, May 1976.

[10]Hodges, D. H., "Nonlinear Equations for the Dynamics of Pretwisted Beams Undergoing Small Strains and Large Rotations," NASA TP-2470, May 1985.

[11]Fulton, M. V., and Hodges, D. H., "Application of Composite Rotor Blade Stability Analysis to Extension-Twist Coupled Blades," *Proceedings of the AIAA/ASME/ASCE/AHS/ ACS 33rd Structures, Structural Dynamics, and Materials Conference* (Dallas, TX), AIAA, Washington, DC, 1992, pp. 1989–1995 (AIAA Paper 92-2254).

[12]Fulton, M. V., and Hodges, D. H., "Aeroelastic Stability of Composite Hingeless Rotor Blades in Hover—Part I: Theory," *Mathematical and Computer Modelling*, Vol. 18, No. 3/4, 1993, pp. 1–18.

[13]Fulton, M. V., and Hodges, D. H., "Aeroelastic Stability of Composite Hingeless Rotor Blades in Hover—Part II: Results," *Mathematical and Computer Modelling*, Vol. 18, No. 3/4, 1993, pp. 19–36.

[14]Friedmann, P. P., and Straub, F. K., "Application of the Finite Element Method to Rotary Wing Aeroelasticity," *Journal of the American Helicopter Society*, Vol. 25, Jan. 1980, pp. 36–44.

[15]Sivaneri, N. T., and Chopra, I., "Dynamic Stability of a Rotor Blade Using Finite Element Analysis," *AIAA Journal*, Vol. 20, No. 5, 1982, pp. 716–723.

[16]Hong, C. H., and Chopra, I., "Aeroelastic Stability Analysis of a Composite Rotor Blade," *Journal of the American Helicopter Society*, Vol. 30, April 1985, pp. 57–67.

[17]Kocurek, J. D., and Tangler, J. L., "A Prescribed Wake Lifting Surface Hover Performance Analysis," *Journal of the American Helicopter Society*, Vol. 22, Jan. 1977, pp. 24–35.

[18]Landgrebe, A. J., "The Wake Geometry of a Hovering Helicopter Rotor and Its Influence on Rotor Performance," *Journal of the American Helicopter Society*, Vol. 17, Oct. 1972, pp. 3–15.

[19]Bauchau, O. A., and Hong, C. H., "Nonlinear Composite Beam Theory," *Journal of Applied Mechanics*, Vol. 55, March 1988, pp. 156–163.

[20]Cho, M. H., and Lee, I., "Aeroelastic Stability of Hingeless Rotor Blade in Hover Using Large Deflection Theory," *AIAA Journal*, Vol. 32, No. 7, 1994, pp. 1472–1477.

[21]Kats, J., and Plotkin, A., *Low Speed Aerodynamics—from Wing Theory to Panel Method*, McGraw–Hill, New York, 1991, pp. 479–495.

[22]Johnson, W., *Helicopter Theory*, Princeton Univ. Press, Princeton, NJ, 1980, pp. 349–361.

[23]Yoo, K. M., "Prediction of Rotor Unsteady Airloads Using Vortex Filament Theory," *Proceedings of the 10th AIAA Applied Aerodynamics Conference* (Palo Alto, CA), AIAA, Washington, DC, 1992, pp. 85–99 (AIAA Paper 92-2610).

[24]Hammond, C. E., and Doggett, R. V., Jr., "Determination of Subcritical Damping by Moving-Block/Randomdec Application," NASA Symposium on Flutter Testing Techniques, Oct. 1975.

[25]Caradona, F. X., and Tung, C., "Experimental and Analytical Studies of a Helicopter Rotor in Hover," NASA TM-81232, 1981.

Recommended Reading from Progress in Astronautics and Aeronautics

**Propagation of Intensive Laser Radiation in Clouds**

O.A. *Volkovitsky*, Yu.S. *Sedunov*, *and* L.P. *Semenov*

This text deals with the interaction between intensive laser radiation and clouds and will be helpful in implementing specific laser systems operating in the real atmosphere. It is intended for those interested in the problems of laser radiation propagation in the atmosphere and those specializing in non-linear optics, laser physics, and quantum electronics. Topics include: Fundamentals of Interaction Between Intense Laser Radiation and Cloud Medium; Evaporation of Droplets in an Electromagnetic Field; Radiative Destruction of Ice Crystals; Formation of Clearing Zone in Cloud Medium by Intense Radiation; and more.

1992, 339 pps, illus, Hardback
ISBN 1-56347-020-9
AIAA Members $59.95
Nonmembers $92.95
Order #: V-138 (830)

**Place your order today! Call 1-800/682-AIAA**

AIAA
American Institute of Aeronautics and Astronautics
Publications Customer Service, 9 Jay Gould Ct., P.O. Box 753, Waldorf, MD 20604
FAX 301/843-0159 Phone 1-800/682-2422 8 a.m. - 5 p.m. Eastern

Sales Tax: CA residents, 8.25%; DC, 6%. For shipping and handling add $4.75 for 1-4 books (call for rates for higher quantities). Orders under $100.00 must be prepaid. Foreign orders must be prepaid and include a $20.00 postal surcharge. Please allow 4 weeks for delivery. Prices are subject to change without notice. Returns will be accepted within 30 days. Non-U.S. residents are responsible for payment of any taxes required by their government.